Available online at www.sciencedirect.com
ScienceDirect
Trans. Nonferrous Met. Soc. China 25(2015) 3729−3735
Transactions of Nonferrous Metals Society of China
www.tnmsc.cn

Electrochemical hydrogen storage properties of non-equilibrium $Ti_{2-x}Mg_xNi$ alloys

Jia-jia LI[1], Jun-feng ZHOU[1], Xiang-yu ZHAO[1], Meng YANG[1], Li-qun MA[1], Xiao-dong SHEN[1,2]

1. College of Materials Science and Engineering, Nanjing Tech University, Nanjing 210009, China;
2. State Key Laboratory of Materials-Oriented Chemical Engineering, Nanjing Tech University, Nanjing 210009, China

Received 15 December 2014; accepted 4 May 2015

Abstract: Amorphous $Ti_{2-x}Mg_xNi$ (x=0−0.3) alloys were prepared by mechanical milling of elemental powders. Charge and discharge test, linear polarization (LP) and potential-step measurement were carried out to investigate the electrochemical hydrogen storage properties of the alloys before and after heat treatment. The results show that the maximum discharge capacity of heat-treated $Ti_{2-x}Mg_xNi$ alloy can reach 275.3 mA·h/g, which is 100 mA·h/g higher than that of the amorphous $Ti_{2-x}Mg_xNi$ alloy. The heat-treated $Ti_{1.9}Mg_{0.1}Ni$ alloy presents the best cycling stability with a high discharge capacity of 210 mA·h/g after 30 cycles. The results of LP and potential-step measurement of the $Ti_{1.9}Mg_{0.1}Ni$ alloy show that the exchange current density increases from 101.1 to 203.3 mA/g and the hydrogen diffusion coefficient increases from 3.20×10^{-11} to 2.70×10^{-10} cm^2/s after the heat treatment, indicating that the heat treatment facilitates both the charge-transfer and hydrogen diffusion processes, resulting in an improvement in electrochemical hydrogen storage properties of $Ti_{2-x}Mg_xNi$ (x=0−0.3) alloys.

Key words: $Ti_{2-x}Mg_xNi$ alloy; amorphous; heat treatment; exchange current density; hydrogen diffusion coefficient

1 Introduction

Nickel/metal hydride (Ni/MH) secondary batteries have been widely researched for their high capacity, long cycle life, non-toxic and environmentally friendly features [1,2]. The performance of Ni/MH batteries mainly depends on the electrochemical hydrogen storage properties of negative materials, such as discharge capacity, activation performance, discharge potential characteristic, cycle life and rate dischargeability [3−7]. To date, the negative materials can be principally classified as AB_5-type alloys, AB_2-type alloys, AB-type alloys, AB_3-type alloys, A_2B_7-type alloys, Mg-based alloys and V-based solid solution alloys [8−14]. $LaNi_5$-based, La−Mg−Ni-based and Zr−Ti−V-based alloys have been commercialized [11,15,16]. However, high price and complex production craft hinder their large-scale commercial application. Thus, seeking a low-cost and simple preparation method of hydrogen storage alloy is imperative.

Ti_2Ni alloy has attracted more attention as the hydrogen storage material for its high theoretical hydrogen storage capacity of 500 mA·h/g [17−19]. However, the formation of irreversible metal hydride during hydrogen absorption and the corrosion in the alkaline electrolyte limit the application of Ti_2Ni alloy [17,18]. In order to improve the discharge performance of Ti_2Ni alloy, many strategies regarding to elemental substitution and structural refinement have been performed. LUAN et al [20] and WANG et al [21] showed that the cycling stability of Ti_2Ni electrode was improved significantly with the substitution of cobalt or palladium for nickel. HU et al [22] proposed that vanadium substitution for titanium contributed to a capacity retention rate of 80% after 30 cycles [22]. Compared with high price of the above-mentioned substitution elements (Co, Pd and V), the use of abundant and low cost magnesium, which has a high hydrogen storage capacity (the mass fraction of 7.6% or approximately 2200 mA·h/g) [23], for the substitution would be of great interest. However, this has not yet been reported in the Ti_2Ni-type system. Apart from the element substitution, the bulk structure also plays an

Foundation item: Project (51201089) supported by the National Natural Science Foundation of China; Project supported by the Priority Academic Program Development (PAPD) of Jiangsu Higher Education Institutions of China
Corresponding author: Xiang-yu ZHAO; E-mail: xiangyu.zhao@njtech.edu.cn
DOI: 10.1016/S1003-6326(15)64016-X

important role in the electrochemical performance of hydrogen storage alloys. For instance, ZHAO et al [24] reported that the amorphous Ti_2Ni alloy had a high capacity retention rate of 80.8% after 50 cycles, which was 47.8% higher than that of crystalline Ti_2Ni alloy.

In this study, amorphous $Ti_{2-x}Mg_xNi$ alloys were prepared by mechanical milling and then heat-treated at 683 K. The structure and electrochemical performance of non-equilibrium $Ti_{2-x}Mg_xNi$ alloys were investigated.

2 Experimental

Powders of Ti (99.9% purity, ~75 μm), Ni (99.99% purity, ~75 μm) and Mg (99.99% purity, ~75 μm) were mixed together to form a nominal composition of $Ti_{2-x}Mg_xNi$ (x=0, 0.1, 0.2, 0.3). The powders were loaded into a stainless steel container and milled at a speed of 350 r/min on a planetary ball mill (QM−3SP2, Nanjing) under argon atmosphere for 100 h. The mass ratio of ball to powder was 20:1. The as-prepared powders were heat-treated in a tube furnace at 683 K under the argon atmosphere. The structure and morphology of the ball milled products were characterized by X-ray diffraction (XRD, Cu K_α radiation) and scanning electron microscopy (SEM, JSM−5900).

The charge and discharge test was conducted in a half-cell consisting of a Ti−Mg−Ni working electrode, a $Ni(OH)_2$/NiOOH counter electrode, and a Hg/HgO reference electrode in a 6 mol/L KOH solution in a BT−2000 testing equipment (Arbin, USA). The details of charge and discharge testing were described in the previous study [24]. Liner polarization (scan rate of 1 mV/s, potential range of −10 to 10 mV versus the open circuit potential) and potential-step measurement (a potential-step between the open circuit potential and −0.6 V versus the reference electrode for 7200 s) were performed on a CHI 660D workstation at 298 K.

3 Results and discussion

3.1 Structure and morphology of amorphous $Ti_{2-x}Mg_xNi$ alloys

Figure 1(a) shows the XRD patterns of Ti_2Ni powders milled for different periods. After 10 h of milling, the intensities of diffraction peaks corresponding to the raw materials are drastically weakened. The diffraction peaks of nickel and titanium almost disappear by 30 h of milling and the Bragg peaks are broadened further with an increase of milling time. The powders predominantly exhibit the amorphous phase after being milled for 100 h. Figure 1(b) shows the XRD patterns of $Ti_{2-x}Mg_xNi$ (x=0−0.3) powders by 100 h of milling, which indicates that the amorphous structure remains by magnesium substitution for titanium. Figure 2 shows the morphologies of $Ti_{2-x}Mg_xNi$ (x=0−0.3) alloy powders milled for 100 h. When x=0.1, the alloy powders show a similar particle size with amorphous Ti_2Ni powders. Whereas, when x increases to 0.2, the fracture process plays an important role in the mechanical alloying of $Ti_{2-x}Mg_xNi$ powders, bringing about a distinct reduce in particle size.

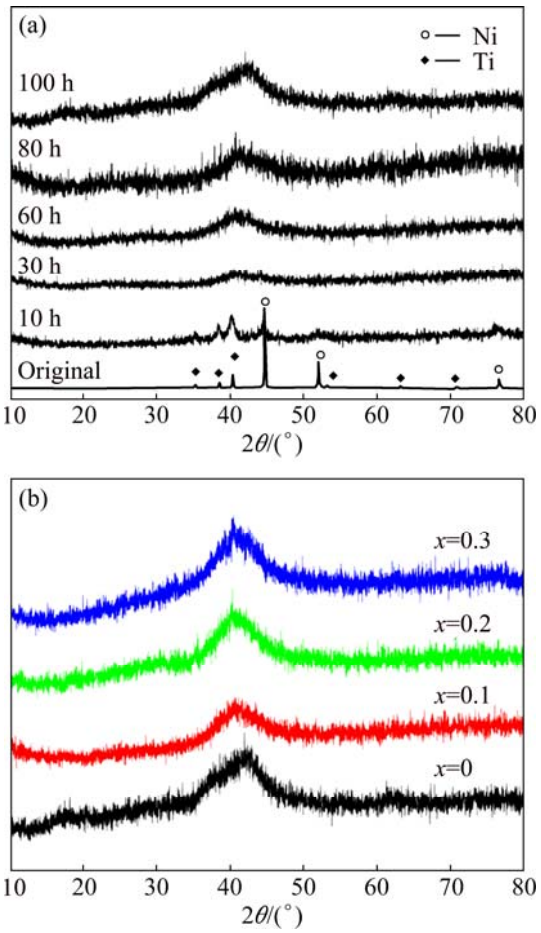

Fig. 1 XRD patterns of Ti_2Ni powders milled for different periods (a) and amorphous$Ti_{2-x}Mg_xNi$ (x=0−0.3) alloys milled for 100 h (b)

3.2 Electrochemical hydrogen storage properties of amorphous $Ti_{2-x}Mg_xNi$ alloys

Figure 3(a) shows the discharge capacities of the amorphous $Ti_{2-x}Mg_xNi$ (x=0−0.3) electrodes as a function of cycle number at a current density of 60 mA/g. All the alloys show good activation performance. The maximum discharge capacities (C_{max}) of $Ti_{2-x}Mg_xNi$ (x=0.1, 0.2, 0.3) are 156.2, 169.1 and 180.6 mA·h/g, respectively, which are higher than 147.5 mA·h/g of the amorphous Ti_2Ni electrode. However, the capacity retention rates after 50 cycles (S_{50}) of $Ti_{2-x}Mg_xNi$ (x=0.1, 0.2, 0.3) electrodes were lower than that of the amorphous Ti_2Ni alloy, as shown in Table 1. Moreover, the cycling stability of the alloys gets worse with the

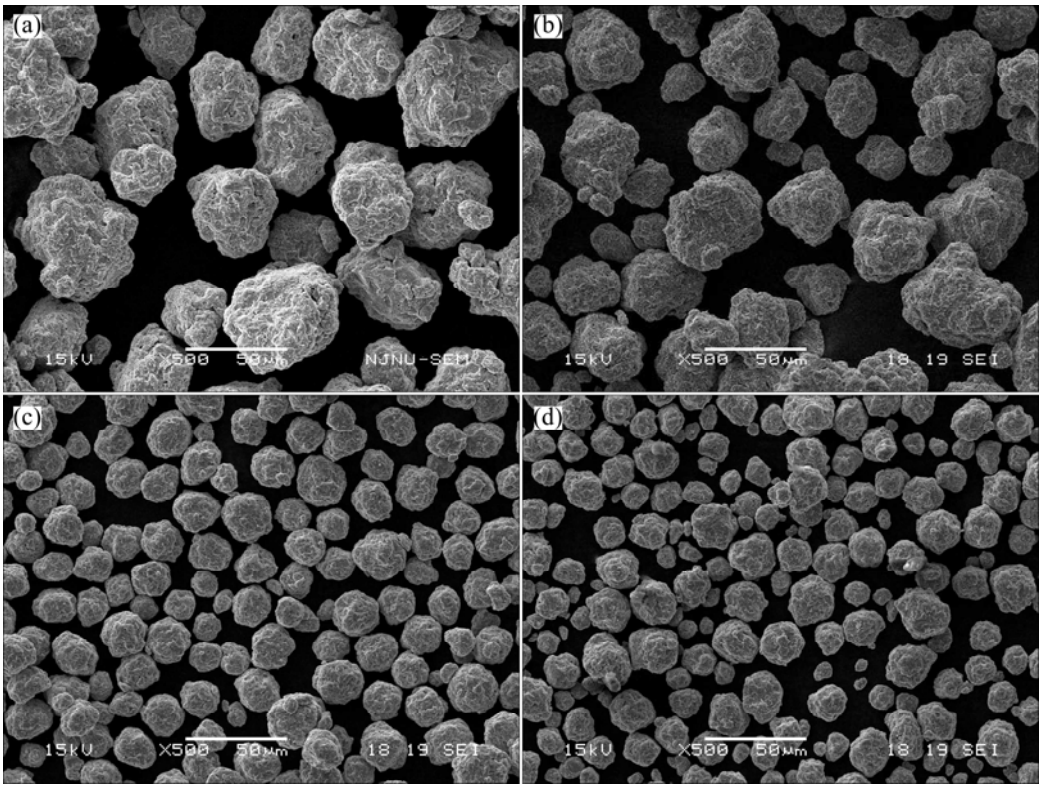

Fig. 2 SEM images of amorphous $Ti_{2-x}Mg_xNi$ (x=0−0.3) alloys milled for 100 h with x values of 0 (a), 0.1 (b), 0.2 (c) and 0.3 (d)

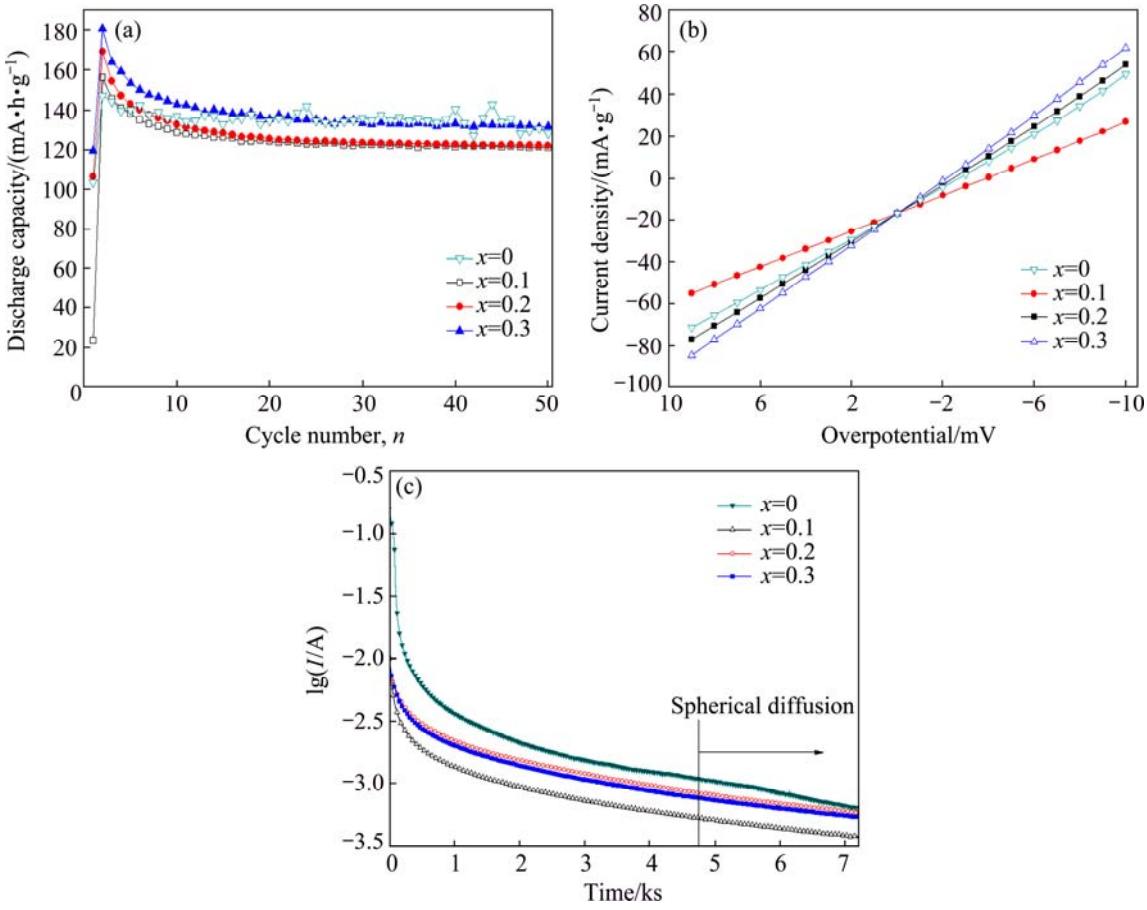

Fig. 3 Cycling stability at current density of 60 mA/g (a), linear polarization curves (b) and semi-logarithmic plots of anodic current versus time response (c) of amorphous $Ti_{2-x}Mg_xNi$ (x=0, 0.1, 0.2, 0.3) electrodes

Table 1 Electrochemical data of amorphous $Ti_{2-x}Mg_xNi$ (x=0, 0.1, 0.2, 0.3) alloys

x	Average particle size/μm	C_{max}/ (mA·h·g^{-1})	S_{50}/%	J_0/ (mA·g^{-1})	D/ (10^{-11}cm^2·s^{-1})
0	21	147.5	92.5	147.5	8.34
0.1	15	156.2	77.6	101.1	3.20
0.2	10	169.1	73.1	161.5	2.87
0.3	10	180.6	72.2	181.1	2.38

increase of magnesium content. This may be due to the corrosion of magnesium in alkaline solution to form loose $Mg(OH)_2$ layer [25].

The electrochemical performance of hydrogen storage alloys is determined by both the reaction on the alloy/electrolyte interface and the hydrogen diffusion within the bulk alloy. The exchange current density (J_0) and hydrogen diffusion coefficient (D) are important parameters for the electrochemical hydrogen storage performance. Figure 3(b) shows the linear polarization curves of amorphous $Ti_{2-x}Mg_xNi$ (x=0−0.3) alloys. The exchange current density (J_0) can be evaluated by linearizing the conventional Butler–Volmer equation at low overpotential regions (<20 mV) [26]. The equation is written as follows:

$$J_0 = \frac{J_a RT}{F\eta} \tag{1}$$

where J_a is the applied current density (mA/g), R is the gas constant (8.314 J/K), T is the absolute temperature, F is the Faraday constant (96485 C/mol) and η is the overpotential of the electrochemical reaction for the hydrogen storage alloy. The values of J_0 were listed in Table 1. The exchange current density decreases first and then increases with the increase of magnesium content. It is well known that the larger the exchange current density is, the better the charge transfer capability is [27]. Both the surface composition and the particle size of alloy powders affect the charge transfer capability. The hydrogen dissociation ability on the magnesium surface is inferior to that on the transition metals [28], and thus the exchange current density of amorphous $Ti_{1.9}Mg_{0.1}Ni$ alloy is smaller than that of Ti_2Ni. When the magnesium substitution increases to 0.2 or 0.3, the particle size of alloy powders decreases drastically, resulting in an increase of specific surface area of the alloy. Therefore, the exchange current density of the alloy increases to 161.5 (x=0.2) and 181.1 mA/g (x=0.3). The magnesium substitution improved the charge transfer reaction of $Ti_{2-x}Mg_xNi$ (x=0.2, 0.3) alloys.

Figure 3(c) presents the semi-logarithmic plots of the anodic current versus the time response of amorphous $Ti_{2-x}Mg_xNi$ (x=0, 0.1, 0.2, 0.3) electrodes. When the test time is above 4700 s, all the plots show a linear relationship and then the average hydrogen diffusion coefficient D of the electrode can be calculated by the following equation [29]:

$$\lg J_d = \lg\left(\frac{6FD}{\rho a^2}(C_0 - C_s)\right) - \frac{\pi^2}{2.303}\frac{D}{a^2}t \tag{2}$$

where J_d is the diffusion current density (A/g), ρ is the density of the hydrogen storage alloy (g/cm^3), a is the average radius of the particles (cm), C_0 is the initial hydrogen concentration in the bulk of the alloy (mol/cm^3), C_S is the hydrogen concentration on the surface of the alloy particle (mol/cm^3), and t is the discharge time (s). The hydrogen diffusion coefficients D of amorphous $Ti_{2-x}Mg_xNi$ (x= 0, 0.1, 0.2, 0.3) electrodes were calculated and are listed in Table 1. With the increase of magnesium content, the hydrogen diffusion within the alloy is hindered. The hydrogen diffusion coefficient in metal depends on the interaction between metal and hydrogen as well as the hydrogen concentration within the metal powder bulk [30−32]. Magnesium is an element for the formation of a strong hydride, which is too stable to desorb hydrogen. When the magnesium content is higher, more hydrogen is easy to be absorbed, leading to an increase of the discharge capacity. However, this also limits the hydrogen desorption kinetics, causing a reduction in hydrogen diffusion coefficient. Herein, the magnesium substitution improves the charge transfer process on the alloy/electrolyte interface but declines the hydrogen diffusion process within the bulk alloy. The increase of discharge capacity after magnesium submission is owing to the dominant process of the charge transfer during hydrogen desorption.

3.3 Effect of heat-treatment on electrochemical hydrogen storage properties of $Ti_{2-x}Mg_xNi$ alloys

Figure 4(a) shows the discharge capacities of heat-treated $Ti_{2-x}Mg_xNi$ (x=0−0.3) alloys as a function of cycle number. The maximum discharge capacity of heat-treated $Ti_{2-x}Mg_xNi$ alloys can reach 275.3 mA·h/g, which is much higher than that of the amorphous $Ti_{2-x}Mg_xNi$ (x=0−0.3) alloys. After 30 cycles, the capacity retention rate of the heat-treated $Ti_{1.9}Mg_{0.1}Ni$ alloy can reach 80.2%, which is higher than that of the amorphous $Ti_{1.9}Mg_{0.1}Ni$ alloy (77.6%) listed in Table 1. The heat-treated $Ti_{1.9}Mg_{0.1}Ni$ alloy shows a discharge capacity of 210 mA·h/g, which is 80 mA·h/g higher than that of the amorphous $Ti_{1.9}Mg_{0.1}Ni$ alloy. Consequently, heat treatment significantly improves the electrochemical properties of $Ti_{2-x}Mg_xNi$ (x=0−0.3) alloys [24]. However, a further increase of magnesium content leads to serious capacity decay of the alloys after heat treatment. Figure 4(b) shows the XRD patterns of $Ti_{2-x}Mg_xNi$ (x=0−0.3) alloys after heat treatment at 683 K for 0.5 h. The

heat-treated $Ti_{1.9}Mg_{0.1}Ni$ alloy shows a crystalline structure with a grain size of 48.9 nm, which is assigned to Ti_2Ni phase. Partial amorphous phase still remains. The magnesium substitution does not change the structure of Ti_2Ni alloy. When x is 0.3, the $Ti_{1.7}Mg_{0.3}Ni$ alloy still possesses an amorphous structure. This means that magnesium substitution contributes to the increase of stability of amorphous Ti_2Ni phase.

Figure 5 shows the SEM images of heat-treated $Ti_{2-x}Mg_xNi$ (x=0, 0.1, 0.2, 0.3) alloys after 30 cycles. There is no significant change on the surface of alloys with x values of 0.1 and 0.2. When x increases to 0.3, some cracks form in the alloy powder after repeated hydrogen absorption/desorption. This is probably due to the fact that the magnesium substitution may reduce the toughness of the Ti_2Ni alloy, leading to pulverization of the alloy powders, which accelerates the corrosion of the alloy powders in the electrolyte. Consequently, the discharge capacity of the $Ti_{1.7}Mg_{0.3}Ni$ electrode fades fast. The $Ti_{1.9}Mg_{0.1}Ni$ alloy possesses the best electrochemical performance.

Figure 6(a) shows the discharge curves of $Ti_{1.9}Mg_{0.1}Ni$ alloys before and after the heat treatment at the second cycle. After the heat treatment, the discharge capacity of $Ti_{1.9}Mg_{0.1}Ni$ alloys increases by 120 mA·h/g. Moreover, the $Ti_{1.9}Mg_{0.1}Ni$ alloy shows a distinct discharge plateau after the heat treatment. The linear polarization test of $Ti_{1.9}Mg_{0.1}Ni$ alloys before and after

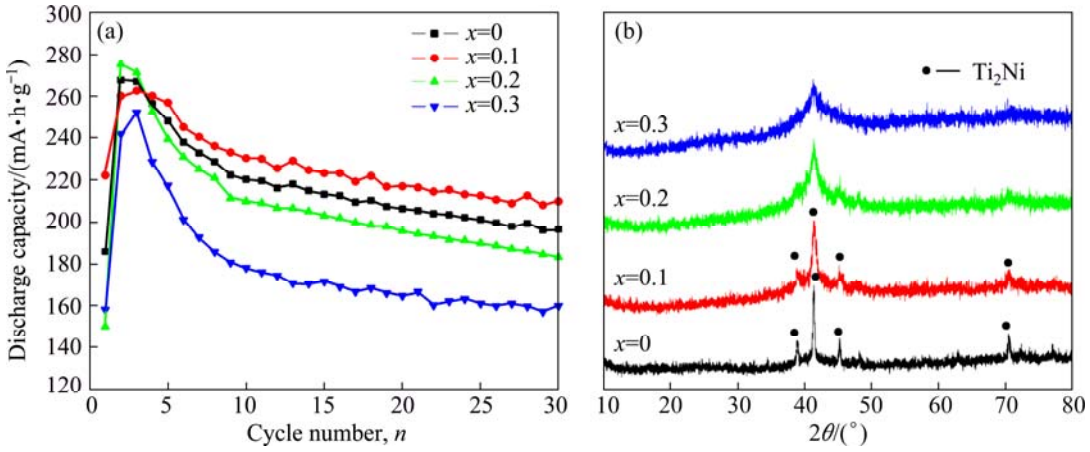

Fig. 4 Discharge capacities of heat-treated $Ti_{2-x}Mg_xNi$ (x=0, 0.1, 0.2, 0.3) alloys as function of cycle number (a) and XRD patterns of $Ti_{2-x}Mg_xNi$ (x=0, 0.1, 0.2, 0.3) alloys after heat treatment at 683 K for 0.5 h (b)

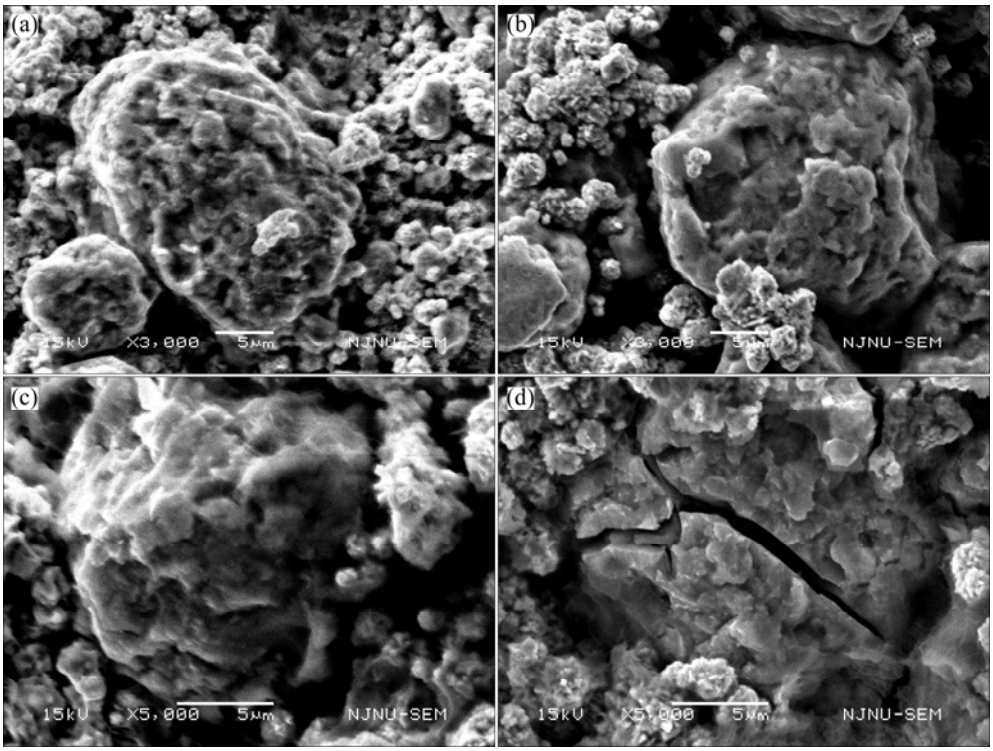

Fig. 5 SEM images of heat-treated $Ti_{2-x}Mg_xNi$ (x=0, 0.1, 0.2, 0.3) alloys after 30 cycles with x values of 0 (a), 0.1 (b), 0.2 (c) and 0.3 (d)

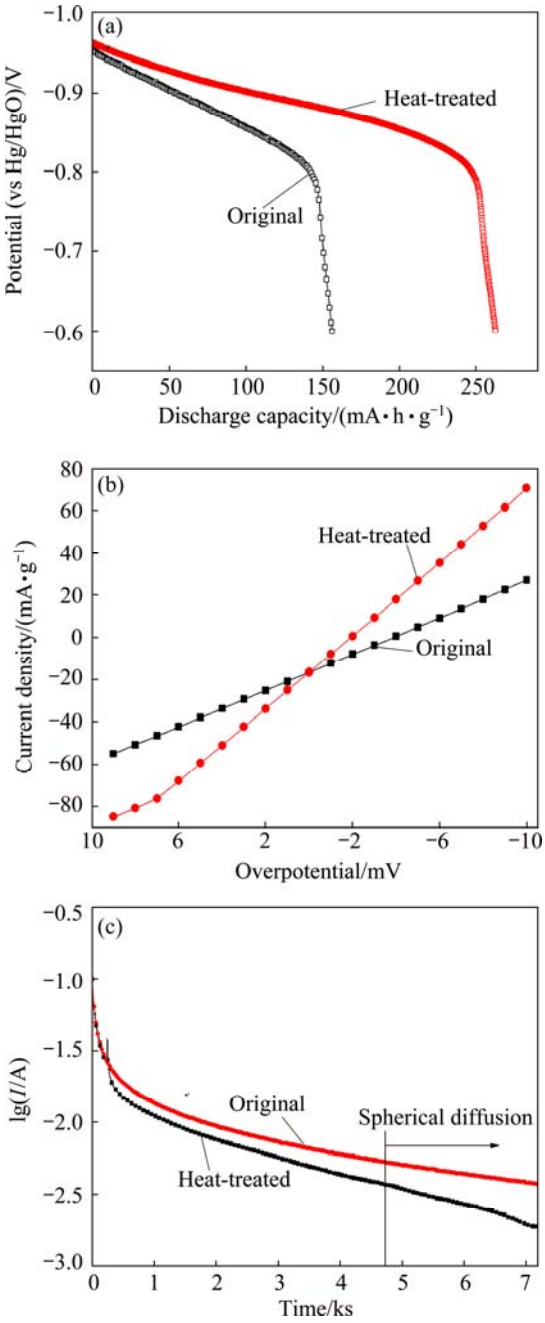

Fig. 6 Discharge curves (a), linear polarization curves (b) and semi-logarithmic plots of anodic current versus time response (c) of $Ti_{1.9}Mg_{0.1}Ni$ alloys before and after heat-treatment at second cycle

the heat treatment was carried out, as shown in Fig. 6(b). The exchange current density of the alloy increases from 101.1 to 203.3 mA/g after the heat treatment. This means that the heat treatment contributes a significant improvement on the charge transfer reaction on the alloy surface. Figure 6(c) shows the result of the potential-step measurement for the $Ti_{1.9}Mg_{0.1}Ni$ alloys before and after the heat treatment. The hydrogen diffusion coefficient of the $Ti_{1.9}Mg_{0.1}Ni$ alloy increases from 3.20×10^{-11} to 2.70×10^{-10} cm^2/s after the heat treatment. The heat treatment induced structure rearrangement of $Ti_{1.9}Mg_{0.1}Ni$ alloys and the trapping of hydrogen by dislocations formed during mechanical milling is avoided [33]. Consequently, the driving force of hydrogen diffusion from the internal to the surface of alloy accelerates.

4 Conclusions

1) Mechanical milling was used to prepare amorphous $Ti_{2-x}Mg_xNi$ (x=0, 0.1, 0.2, 0.3) alloys. The magnesium substitution increases the discharge capacities of $Ti_{2-x}Mg_xNi$ (x=0−0.3) alloys.

2) After the heat treatment, the nanocrystalline $Ti_{1.9}Mg_{0.1}Ni$ alloy presents the best cycling stability with a high discharge capacity of 210 mA·h/g after 30 cycles. The maximum discharge capacity of heat-treated $Ti_{1.8}Mg_{0.2}Ni$ alloy reaches 275.3 mA·h/g, which is higher than that of crystalline Ti_2Ni alloy.

3) The formation of nanocrystalline $Ti_{1.9}Mg_{0.1}Ni$ alloy by the heat treatment contributes a significant improvement on the electrochemical hydrogen storage performance of the $Ti_{2-x}Mg_xNi$ alloy.

4) Compared with amorphous $Ti_{1.9}Mg_{0.1}Ni$ alloy, the exchange current density of the nanocrystalline $Ti_{1.9}Mg_{0.1}Ni$ alloy increases from 101.1 to 203.3 mA/g and the hydrogen diffusion coefficient of the nanocrystalline $Ti_{1.9}Mg_{0.1}Ni$ alloy increases from 3.20×10^{-11} to 2.70×10^{-10} cm^2/s.

References

[1] ZHAO X Y, MA L Q. Recent progress in hydrogen storage alloys for nickel/metal hydride secondary batteries [J]. Int J Hydrogen Energy, 2009, 34(11): 4788−4796.

[2] TIAN X, YUN G H, WANG H Y, SHANG T, YAO Z Q, WEI W, LIANG X X. Preparation and electrochemical properties of La−Mg−Ni-based $La_{0.75}Mg_{0.25}Ni_{3.3}Co_{0.5}$ multiphase hydrogen storage alloy as negative material of Ni/MH battery [J]. Int J Hydrogen Energy, 2014, 39(16): 8474−8481.

[3] ZHAO X Y, MA L Q, GAO Y J, DING Y, SHEN X D. Effect of surface treatments on microstructure and electrochemical properties of La−Ni−Al hydrogen storage alloy [J]. Int J Hydrogen Energy, 2009, 34(4): 1904−1909.

[4] LIU Y F, PAN H G, GAO M X, WANG Q D. Advanced hydrogen storage alloys for Ni/MH rechargeable batteries [J]. J Mater Chem, 2011, 21, 4743−4755.

[5] FAN Y P, PENG X Y, LIU B Z, ZHANG B Q, PENG Q M, JI L Q. Microstructures and electrochemical hydrogen storage performances of $La_{0.75}Ce_{0.25}Ni_{3.80}Mn_{0.90}Cu_{0.30}(V_{0.81}Fe_{0.19})_x$ (x=0−0.20) alloys [J]. Int J Hydrogen Energy, 2014, 39(13): 7042−7049.

[6] WANG L, YAN H Z, XIONG W, LI B Q, LI J, KONG F Q. The influence of boron content on the structural and electrochemical properties of the $La_{15}Fe_{77}B_8$-type hydrogen storage alloy [J]. J Power Sources, 2014, 259: 213−218.

[7] PENG X Y, LIU B Z, FAN Y P, JI L Q, ZHANG B Q, ZHANG Z. Microstructures and electrochemical characteristics of $La_{0.7}Ce_{0.3}Ni_{4.2}Mn_{0.9-x}Cu_{0.37}(V_{0.81}Fe_{0.19})_x$ hydrogen storage alloys [J]. Electrochim Acta, 2013, 93: 207−212.

[8] YAO Q R, ZHOU H Y, WANG Z M, PAN S K, RAO G H. Electrochemical properties of the $LaNi_{4.5}Co_{0.25}Al_{0.25}$ hydrogen

storage alloy in wide temperature range [J]. J Alloy Compd, 2014, 606: 81−85.
[9] PENG X Y, LIU B Z, FAN Y P. Microstructures and electrochemical hydrogen storage characteristics of $La_{0.7}Ce_{0.3}Ni_{4.2}Mn_{0.9-x}Cu_{0.37}$-$(Fe_{0.43}B_{0.57})_x$ (x=0−0.20) alloys [J]. J Power Sources, 2013, 240: 178−183.
[10] LI X D, ELKEDIMA O, NOWAK M, JURCZYK M. Characterization and first principle study of ball milled Ti–Ni with Mg doping as hydrogen storage alloy [J]. Int J Hydrogen Energy, 2014, 39(18): 9735−9743.
[11] LIU W Q, WANG X L, HU W, KAWABE Y, WTADA M, WANG L M. Electrochemical performance of TiVNi-quasicrystal and AB_3-type hydrogen storage alloy composite materials [J]. Int J Hydrogen Energy, 2011, 36(1): 616−620.
[12] ZHANG Y H, CAI Y, YANG T, HOU Z H, ZHANG G F, ZHAO D L. Influence of melt spinning on the electrochemical hydrogen storage kinetics of RE−Mg−Ni-based A_2B_7-type alloys [J]. Rare Metal Mat Eng, 2013, 42(11): 2201−2206.
[13] ZHANG Y H, WANG H T, YANG T, ZHAI T T, ZHANG G F, ZHAO D L. Electrochemical hydrogen storage performances of the nanocrystalline and amorphous $(Mg_{24}Ni_{10}Cu_2)_{100-x}Nd_x$ (x=0−20) alloys applied to Ni−MH battery [J]. J Rare Earth, 2013, 31(12): 1175−1182.
[14] GAO M X, ZHANG S C, MIAO H, LIU Y F, PAN H G. Pulverization mechanism of the multiphase Ti−V-based hydrogen storage electrode alloy during charge/discharge cycling [J]. J Alloy Compd, 2010, 489: 552−557.
[15] KARWOWSKA M, JARON T, FIJALKOWSKI K J, LESZCZYNSKI P J, ROGULSKI Z, CZERWINSKI A. Influence of electrolyte composition and temperature on behaviour of AB_5 hydrogen storage alloy used as negative electrode in Ni−MH batteries [J]. J Power Sources, 2014, 263: 304−309.
[16] ZHANG Y L, LI J S, ZHANG T B, HU R, XUE X Y. Microstructure and hydrogen storage properties of non-stoichiometric Zr−Ti−V Laves phase alloys [J]. Int J Hydrogen Energy, 2013, 38(34): 14675−14684.
[17] LUAN B, KENNEDY S J, LIU H K, DOU S X. On the charge/discharge behavior of Ti_2Ni electrode in 6 M KOH aqueous and deuterium oxide solutions [J]. J Alloy Compd, 1998, 267: 224−230.
[18] ANIK M, BAKSAN B, ORBAY T O, KUCUKDEVECI N, AYBAR A B, OZDEN R C, GASAN H, KOC N. Hydrogen storage characteristics of Ti_2Ni alloy synthesized by the electro-deoxidation technique [J]. Intermetallics, 2014, 46: 51−55.
[19] LI X D, ELKEDIM O, NOWAK M, JURCZYK M, CHASSAGNON R. Structural characterization and electrochemical hydrogen storage properties of $Ti_{2-x}Zr_xNi$ (x=0, 0.1, 0.2) alloys prepared by mechanical alloying [J]. Int J Hydrogen Energy, 2013, 38(27): 12126−12132.
[20] LUAN B, CUI N, LIU H K, ZHAO H J, DOU S X. Effect of cobalt addition on the performance of titanium-based hydrogen storage electrodes [J]. J Power Sources, 1995, 55(2): 197−203.
[21] WANG C S, LEI Y Q, WANG Q D. Effect of Nb and Pd on the electrochemical properties of a Ti−Ni hydrogen-storage electrode [J]. J Power Sources, 1998, 70(2): 222−227.
[22] HU W, WANG J L, WANG L D, WU Y M, WANG L M. Electrochemical hydrogen storage in $(Ti_{1-x}V_x)_2Ni$ (x=0.05−0.3) alloys comprising icosahedral quasicrystalline phase [J]. Electrochim Acta, 2009, 54(10): 2770−2773.
[23] SAKINTUNA B, LAMARI-DARKRIM F, HIRSCHER M. Metal hydride materials for solid hydrogen storage: A review [J]. Int J Hydrogen Energy, 2007, 32(9): 1121−1140.
[24] ZHAO X Y, MA L Q, YAO Y, DING Y, SHEN X D. Ti_2Ni alloy: A potential candidate for hydrogen storage in nickel/metal hydride secondary batteries [J]. Energy Environ Sci, 2010, 3: 1316−1321.
[25] CAI Z P, LU D S, LI W S, LIANG Y, ZHOU H B. Study on anodic oxidation of magnesium in 6 M KOH solution by alternative current impedance [J]. Int J Hydrogen Energy, 2009, 34(1): 467−472.
[26] YANG M, ZHAO X Y, DING Y, MA L Q, QU X X, GAO Y J. Electrochemical properties of titanium-based hydrogen storage alloy prepared by solid phase sintering [J]. Int J Hydrogen Energy, 2010, 35(7): 2717−2721.
[27] FENG F, NORTHWOOD D O. Effect of surface modification on the performance of negative electrodes in Ni/MH batteries [J]. Int J Hydrogen Energy, 2004, 29(9): 955−960.
[28] NOBUHARA K, KASAI H, DINO W A, NAKANISHI H. H_2 dissociative adsorption on Mg, Ti, Ni, Pd and La surfaces [J]. Surf Sci, 2004, 566−568: 703−707.
[29] LIN J, LIANG F, WU Y M, LIU W Q, WANG L M. Hydrogen storage properties of $Ti_{1.4}V_{0.6}Ni$+xMg (x=1−3, wt.%) alloys [J]. Int J Hydrogen Energy, 2014, 39(7): 3313−3319.
[30] FENG F, NORTHWOOD D O. Hydrogen diffusion in the anode of Ni/MH secondary batteries [J]. J Powder Sources, 2004, 136(2): 346−350.
[31] ZHAO X Y, MA L Q, DING Y, SHEN X D. Structure evolution and electrochemical hydrogenation behavior of Ti_2Ni [J]. Intermetallic, 2010, 18(5): 1086−1090.
[32] FENG F, HAN J, GENG M, NORTHWOOD D O. Study of hydrogen transport in metal hydride electrodes using a novel electrochemical method [J]. J Electroanal Chem, 2000, 487(2): 111−119.
[33] HANG Z M, XIAO X Z, LI S Q, GE H W, CHEN C P, CHEN L X. Influence of heat treatment on the microstructure and hydrogen storage properties of $Ti_{10}V_{77}Cr_6Fe_6Zr$ alloy [J]. J Alloy Compd, 2012, 529: 128−133.

非平衡态 $Ti_{2-x}Mg_xNi$ 合金的电化学储氢性能

李佳佳[1]，周俊凤[1]，赵相玉[1]，杨 猛[1]，马立群[1]，沈晓冬[1,2]

1. 南京工业大学 材料科学与工程学院，南京 210009；
2. 南京工业大学 材料化学工程国家重点实验室，南京 210009

摘 要：采用机械球磨法制备非晶态的 $Ti_{2-x}Mg_xNi$(x=0−0.3)合金粉末。通过充放电测试、线性极化和电位阶跃等方法研究非平衡态 $Ti_{2-x}Mg_xNi$(x=0−0.3)合金热处理前后的电化学储氢性能。结果表明：热处理后 $Ti_{2-x}Mg_xNi$ 合金的最大放电容量高达 275.3 mA·h/g，比非晶态的 $Ti_{2-x}Mg_xNi$ 合金的放电容量高 100 mA·h/g。$Ti_{1.9}Mg_{0.1}Ni$ 合金的循环稳定性最好，经 30 次循环后的容量保持在 210 mA·h/g。经过热处理的 $Ti_{1.9}Mg_{0.1}Ni$ 合金的交换电流密度从 101.1 mA/g 增大到 203.3 mA/g，氢扩散系数从 3.20×10^{-11} cm^2/s 增大到 2.70×10^{-10} cm^2/s，表明热处理明显促进了电极的电子转移和氢扩散过程，从而提高了 $Ti_{2-x}Mg_xNi$ 合金的电化学储氢性能。

关键词：$Ti_{2-x}Mg_xNi$ 合金；非晶态；热处理；交换电流密度；氢扩散系数

(Edited by Mu-lan QIN)